

Article

Assessing the Efficacy of Whole-Body Titanium Dental Implant Surface Modifications in Inducing Adhesion, Proliferation, and Osteogenesis in Human Adipose Tissue Stem Cells

Federico Ferro ^{1,*}, Federico Azzolin ^{2,†}, Renza Spelat ^{3,†}, Lorenzo Bevilacqua ² and Michele Maglione ²¹ Department of Medical and Biological Sciences, University of Udine, 33100 Udine, Italy² Department of Medical, Surgery and Health Sciences, University of Trieste, 34125 Trieste, Italy³ Neurobiology Sector, International School for Advanced Studies (SISSA), 34136 Trieste, Italy

* Correspondence: ferro.federico@libero.it

† These authors contributed equally to this work.

Abstract: Background: Although the influence of titanium implants' micro-surface properties on titanium discs has been extensively investigated, the research has not taken into consideration their whole-body effect, which may be considered possible using a combinatorial approach. Methods: Five titanium dental implants with a similar moderate roughness and different surface textures were thoroughly characterized. The cell adhesion and proliferation were assessed after adipose-tissue-derived stem cells (ADSCs) were seeded on whole-body implants. The implants' inductive properties were assessed by evaluating the osteoblastic gene expression. Results: The surface micro-topography was analyzed, showing that hydroxyapatite (HA)-blasted and bland acid etching implants had the highest roughness and a lower number of surface particles. Cell adhesion was observed after 24 h on all the implants, with the highest score registered for the HA-blasted and bland acid etching implants. Cell proliferation was observed only on the laser-treated and double-acid-etched surfaces. The ADSCs expressed collagen type I, osteonectin, and alkaline phosphatase on all the implant surfaces, with high levels on the HA-treated surfaces, which also triggered osteocalcin expression on day seven. Conclusions: The findings of this study show that the morphology and treatment of whole titanium dental implants, primarily HA-treated and bland acid etching implants, impact the adherence and activity of ADSCs in osteogenic differentiation in the absence of specific osteo-inductive signals.

Keywords: periodontology; surface chemistry; bone implant interactions; cell-implant interactions

Citation: Ferro, F.; Azzolin, F.; Spelat, R.; Bevilacqua, L.; Maglione, M. Assessing the Efficacy of Whole-Body Titanium Dental Implant Surface Modifications in Inducing Adhesion, Proliferation, and Osteogenesis in Human Adipose Tissue Stem Cells. *J. Funct. Biomater.* **2022**, *13*, 206. <https://doi.org/10.3390/jfb13040206>

Academic Editors: Iulian Vasile Antoniac and Shariq Najeeb

Received: 27 September 2022

Accepted: 25 October 2022

Published: 27 October 2022

Publisher's Note: MDPI stays neutral with regard to jurisdictional claims in published maps and institutional affiliations.



Copyright: © 2022 by the authors. Licensee MDPI, Basel, Switzerland. This article is an open access article distributed under the terms and conditions of the Creative Commons Attribution (CC BY) license (<https://creativecommons.org/licenses/by/4.0/>).

1. Introduction

It is estimated that in 2019, the global dental implant market was worth around 4.6 billion USD, and it is predicted to increase at an annual progression rate of 9.0% from 2020 to 2027 [1]. Healthy people typically recover quickly from dental implant surgery through the repair and regeneration of the surrounding tissues. However, people suffering from pathological conditions, such as osteoporosis or diabetes, experience delays [2].

The effectiveness of the rehabilitation process after implant placement is dependent on appropriate epithelial and bone growth, which allows the device to osseointegrate in the implantation site. The term "osseointegration" refers to the "formation of a direct contact between the dental implant and the living bone" [3]. Fast and tight osseointegration and, therefore, excellent long-term stability are mandatory for dental implants. The most important factor responsible for the stability and duration of an oral implant is likely the macro- and micro-topography of the implant. In fact, properties such as the shape, elasticity, roughness, chemical composition, electric charge, oxide type, and thickness have been demonstrated to play significant roles [4–11]. Theoretically, the surface geometry, charge and their chemical-physical modifications have to fulfill four main tasks: (1) prevent the

unspecific adsorption of denatured proteins at the interface between the oral tissues and implants [12]; (2) attract differentiated or undifferentiated progenitor cells from the native tissue [13]; (3) induce native tissue or progenitor cell regeneration and differentiation [13]; and (4) guarantee an optimal load transfer to the bone [6,14]. Implants are mainly classified into four types based on their surface roughness, as determined by the arithmetical mean of the roughness area (Sa), defined as rough (Sa > 2.0 μm), moderately rough (Sa between 1.0–2.0 μm), minimally rough (Sa between 0.5–1.0 μm), or smooth (Sa < 0.5 μm) [15,16]. Many studies employing stem cells in vivo and in vitro in order to understand the mechanism of osseointegration [17–19] have found that implant titanium discs [20,21] with moderately rough surfaces enable better cell and bone connections than smoother or rougher surfaces [15,16,22–29]. Surface roughness is also linked to favorable effects on load transmission via the distribution of well-tolerated micro-strains, 0.25–0.50 $\mu\epsilon$ [6,30,31], which also favor osteoblastic and progenitor cell differentiation [6,31,32].

Surprisingly, despite being a more realistic and clinically suitable approach [2], little is known about the impact of whole-body implants on stem cells, including their attraction or adhesion and, secondly, their proliferative and differentiation potential. Interestingly, stem cell have recently been identified as a combinatorial tissue engineering strategy that can be used to improve titanium implant osseointegration in diabetic and osteoporotic animal models [2,33].

Among stem cells, adipose-tissue-derived stem cells (ADSCs) are easily accessible and expandable in vitro, and they are capable of anti-inflammatory activity and differentiating between various lineages of paramount importance for implant dentistry, such as osteoblastic, ameloblastic, and odontoblastic lineages [34–37].

In detail, in the present research, we evaluate whether the micro-geometry and surface characteristics of five different whole-body commercially available titanium implants with a roughness between 1 and 2 μm affect the behavior of a population of ADSCs from the point of view of their adhesion, proliferation, and differentiation in vitro.

2. Materials and Methods

2.1. Cell Culture Products and Reagents

According to the ethical committee of the University of Udine, lipoaspirates were collected from healthy donors over the age of 18 after receiving informed consent and adhering to all legal criteria for confidentiality and the management of biological material.

Lipoaspirates (15 mL) were taken from the donors utilizing the tumescent technique based on an infusion of Klein's solution followed by the recovery of the adipose tissue [34]. After that, the adipose tissue was centrifuged at $1800\times g$ for 15 min to eliminate the red blood cells. The ADSCs were placed in Jocklik modified alpha-MEM medium (Gibco, Carlsbad, CA, USA) supplemented with 400 U/mL collagenase type 2 (Worthington, Columbus, OH, USA) equal to two times the volume of lipoaspirates, and the solution was incubated for 15 min at 37 °C, with gentle shaking every 2–3 min [34]. The solution was then centrifuged at $1800\times g$ for 10 min [34]. The supernatant was discarded, and the pellet was resuspended and filtered through a filter to select the cell fractions smaller than 70 μm [34]. The ADSCs were plated onto 100 mm dishes (2×10^6 cells per dish) and cultured in proliferation medium, adapted from Ferro F. et al., composed of α -MEM with L-glutamine 2 mmol/L, 10% fetal bovine serum (FBS), insulin 10 mg/mL, dexamethasone 10^{-9} mol/L, ascorbic acid 100 mM, EGF 10 ng/mL, and gentamicin 50 ng/mL (all from Sigma-Aldrich, Saint Louis, MO, USA) [34]. Colonies developed in the primary culture and reached near confluency within approximately one week. The ADSCs were maintained as semiconfluent to prevent cell differentiation, and approximately 80% of the medium was replaced every three days.

The stem cells derived from adipose tissue were maintained in culture medium at 37 °C, 5% CO₂, in a humidified atmosphere. To detach the ADSCs, a bland detaching solution, namely CTC (collagenase 20 U/mL, trypsin 0.75 mg/mL, 2% heat-inactivated dialyzed chicken serum (Gibco) in Ca and Mg Hank's Balanced Salt Solution (HBSS)), was

used. The cells were maintained in culture from passages one to six (P1 to P6) on 150 mm culture plates and then were used in the experiments [34].

2.2. ADSC Characterization

The following antibodies were used to characterize the P6 ADSC membrane-bound cluster of differentiation stem markers: CD34, CD45, CD73, CD90, CD105, CD106 (BD, Franklin Lakes, NJ, USA), human leukocyte antigen-DR isotype (HLA-DR), IgG1 BD (BD), IgG2b, and IgG1 κ (Invitrogen, Waltham, MA, USA). Briefly, the cells (2.2×10^6 cells) were detached, re-suspended in incubation buffer, and incubated for 1 h at 4 °C with the antibodies. The cells were washed with PBS, centrifuged, and re-suspended in 100 μ L wash buffer before being analyzed. A threshold was established for the forward and side scatter dot plots to exclude the cellular debris, and 20,000 events were analyzed using the Becton-Dickinson (BD) FACS Canto flow cytometer and FlowJo (BD) software.

2.3. Multi-Differentiation Assays

The ADSCs at P6 were differentiated through the osteoblastic, adipocyte, and chondroblastic lineages using the following media composition: F-12 Coon's modified/Ambesi's modified medium (Gibco) supplemented with dexamethasone 100 nM, b-glycerophosphate 1 mM, Ca²⁺ 1.2 mM, Mg²⁺ 0.6 mM, glucose 2 g/L, vitamin K2 1 mM, vitamin D3 5 nM, gentamicin 50 ng/mL, FBS 0.5% (all from Sigma-Aldrich, Saint Louis, MO, USA), retinoic acid 250 nM, 17- β -estrogen 1 mM, and calcitonin 1 nM (all from MP-Biomedicals, Santa Ana, CA, USA). The following components were used to produce the adipogenic induction and maintenance media: DMEM high glucose (HG) (Gibco), 3-isobutyl-1-methyl-xanthine 25 μ M, insulin 10 μ g/mL, dexamethasone 1 μ M, indomethacin 200 μ M, gentamicin 50 ng/mL, FBS 10%, (Sigma-Aldrich), DMEM (HG), FBS 10%, insulin 10 μ g/mL, and gentamicin 50 ng/mL. The chondrogenic medium composition was as follows: DMEM (HG), dexamethasone 100 nM, ascorbic acid 50 μ g/mL, L-proline 40 μ g/mL, insulin 5 μ g/mL, transferrin 5 μ g/mL, selenous acid 5 ng/mL, linoleic acid 5.35 μ g/mL, transforming growth factor-3 (TGF β -3) 10 ng/mL, sodium pyruvate 1 mM, and gentamicin 50 ng/mL (all from Sigma-Aldrich). At day 20, Alizarin Red S (Sigma-Aldrich) staining was used to validate the osteogenic capacity of the ADSCs. Oil Red O (Sigma-Aldrich) was used to measure the adipogenic differentiation on day 21. After 21 days in culture, the degree of chondrogenesis differentiation was assessed by safranin O staining (Sigma-Aldrich).

2.4. Characteristics of the Dental Implants

Five different titanium dental implants were compared in this study, as follows: plasma spray; laser; HA-blasted with hydroxyapatite (HA) and bland acid etching; double acid etching; and HA-blasted with HA followed by "new" patented treatment (Table 1). The plasma-spray-treated implant is made of grade 4 titanium with the overall nominal chemical composition shown in Table 1 [38], and the device is machined automatically before being packaged. The laser-treated implant is made of grade 4 titanium, with the overall nominal chemical composition shown in Table 1 [38]. The implant surface is created through the use of a DPSS Nd Q-switching laser source (solid-state, diode-pumped laser, DPSS, with an Nd source in the Q-sw regime). With this technique, the material is removed from the surface in the form of vapor, and this "cold" ablation has a high repeatability. The DPSS Nd Q-sw laser technology allows us to create perfectly reproducible micrometric porosities in terms of the shape, diameter, and depth, as well as the distribution and spacing. The HA-blasted implant with HA and bland acid etching is made of Ti6Al4V alloy, with the overall nominal chemical composition shown in Table 1 [38]. The implant surface is obtained by means of a blasting process using HA, followed by treatment with a weak acid to remove the excess micro-granules. The use of HA micro-granules during the blasting process aims to obtain a rougher surface. The double-acid-etching-treated implant is made of grade 4 titanium, with the overall nominal chemical composition shown in Table 1 [38]. The implant surface is obtained via a thermal etching process with hydrochloric acid and sulfuric acid. This

process gives rise to numerous irregularities on the surface at distances of about 1–3 μm, distributed between the peaks. Moreover, the presence of micro-pores of a size of about 1–2 μm increases its surface complexity. The HA-blasted implant subsequently subjected to a “new” patented treatment is made of Ti6Al4V alloy, with the overall nominal chemical composition shown in Table 1 [38]. The description of the surface treatment is protected by a patent.

Table 1. Summary of the characteristics of the tested implants. Five different titanium-formed implants with a roughness between 1 and 2 μm and different surface treatments were tested in this study. Nominal chemical composition of the titanium and titanium alloy implants.

Surface Treatment	Plasma Spray	Laser	HA-Blasted and Bland Acid Etching	Double Acid Etching	HA-Blasted “New” under Patent
Composition	Grade 4 titanium	Grade 4 titanium	Ti6Al4V	Grade 4 titanium	Ti6Al4V
Nominal chemical composition [38]	Ti 99%	Ti 99%	Ti 90%	Ti 99%	Ti 90%
	Fe 0.3%	Fe 0.3%	Fe 0.25%	Fe 0.3%	Fe 0.25%
	O 0.4%	O 0.4%	O 0.2% max	O 0.4%	O 0.2% max
	C 0.1%	C 0.1%	C 0.0%	C 0.1%	C 0.0%
	N 0.05%	N 0.05%	N 0.0%	N 0.05%	N 0.0%
	H 0.015%	H 0.015%	H 0.0%	H 0.015%	H 0.0%
	Al 0.0%	Al 0.0%	Al 6.4%	Al 0.0%	Al 6.4%
V 0.0%	V 0.0%	V 4.12%	V 0.0%	V 4.12%	

2.5. Dental Implant and Surface Characterization

Morphological analyses were executed using a scanning electron microscope Quanta250 (SEM, FEI, Hillsboro, OR, USA) in a high vacuum and in secondary electron mode, with 30 kV of tension. The operational distance was fixed in order to acquire an appropriate magnification. The samples were secured on aluminum stubs covered with carbon double-sided tape and consequently gold-sputtered with a Sputter Coater K550X (Emitech, Quorum Technologies Ltd., Laughton, UK).

SEM photomicrographs ($n = 3$, magnification 1500×) were binarized and thresholded before being processed using ImageJ and the nearest distances (ND) plugin (<http://imagej.nih.gov>, USA, accessed on 2 September 2022) to determine the average size of, and distance between, the implant surface particles. Differences in roughness between the implants were assessed using SEM photomicrographs and the SurfCharJ plugin [13] to evaluate the following parameters: the Rq (root mean square deviation), Rsk (skewness of the assessed profile), Rku (kurtosis of the assessed profile), and Ra (arithmetical mean deviation). Imagej was also used to obtain the surface plot and 3D profile differences of the implants [39].

2.6. Dental Implant Seeding with ADSCs

Each dental implant ($n = 3$) was placed in the vertical position on a 96 multi-well plate (Gibco) and placed onto a 150 mm plate to maintain its sterility. The wells were filled with a known amount of proliferation medium (200 μL) and 1.25×10^6 ADSCs. The medium was changed on day one to remove non-adherent cells and also on day three (Figure 1).

2.7. Cell Adhesion and Proliferation

The cell adhesion was assessed on day one. On days three and seven, the cell proliferation on the implant surface was measured ($n = 3$). The cell detachment from the implants was performed after transferring the implants to 1.5 mL conical tubes containing CTC for 10 min at 37 °C in a humid atmosphere with 5% CO₂ (Figure 1). The Neubauer chamber was used to count the cells in triplicate at each time point.

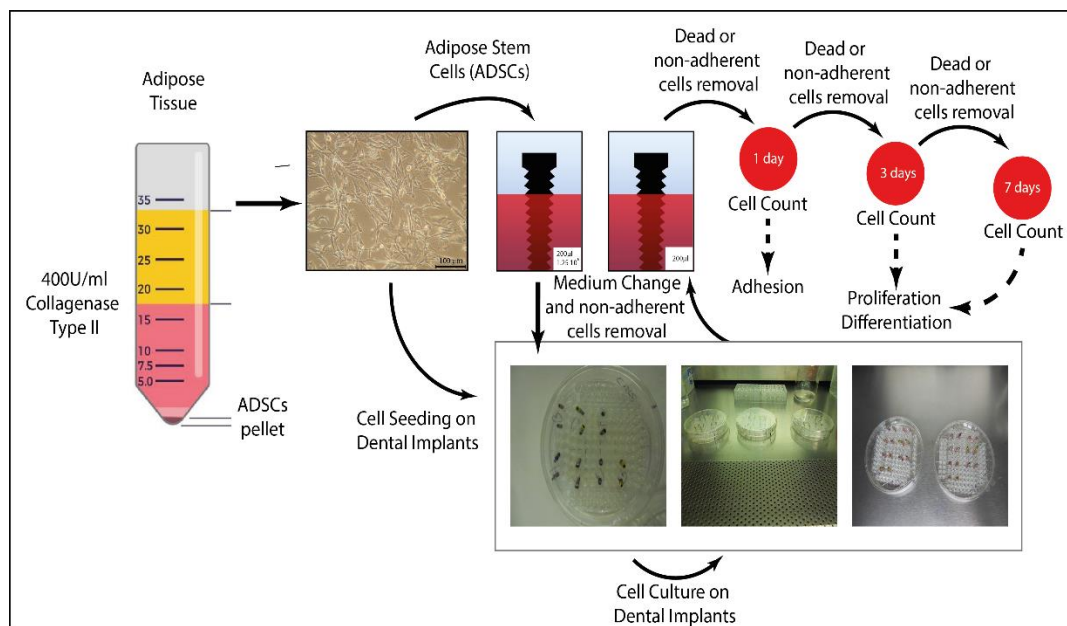


Figure 1. Schematic representation of the seeding and culture phases of the cells on the commercial implants. ADSCs were isolated from lipoaspirates and cultured. Cells were then diluted in proliferation medium and seeded onto whole-body dental implants. Adhesion was assessed on day one, and the proliferation and osteoblastic differentiation were assessed on days three and seven.

2.8. Gene Expression Analysis

The expression of the osteoblastic markers was quantified on days one, three, and seven in triplicate by PCR using the following primers: alkaline phosphatase (ALP) GCAGGCAGGCAGCTTCAC TCAGAACAGGACGCTCAGG, 496 bp, 60.5 °C, NM_000478.3; osteocalcin (Osc) TCACACTCCTCGCCCTATTG CTAGACCGGGCCGTAGAAG, 293 bp, 58 °C, NM_199173.3; osteonectin (Osn) CACAAGTCCACCTGGACTA GAATCCGGTACTGTGGAAGG, 525 bp, 58 °C, NM_003118.2, and collagen Type I (Coll-I) TAAAGGGT-CACCGTGGCT CGAACCACATTGGCATCA, 355 bp, 60 °C, NM_000088.3. RNA polymerase type II GCACCACGTACACCAATG GTGGGGCTGCTTTAACCA, 350 bp, 56 °C, NM_000937, was used as housekeeping gene (MWG Eurofins, Ebersberg, Germany).

2.9. Statistical Analysis

The morphologic and structural variables of the implants, cell counts, and gene expression are expressed as the mean \pm standard deviation. Statistical significance was evaluated by analysis of variance (ANOVA) followed by Fisher's or Bonferroni's post hoc test. The paired *t*-test was used to compare the data obtained from the related groups. SPSS 23.0 (IBM, Armonk, NJ, USA) was used to analyze the data, and statistical significance was defined as $p \leq 0.05$ and $p \leq 0.001$.

3. Results

3.1. ADSC Isolation, Characterization, and Stemness Potential Assessment

We detailed the ADSC isolation methodology in Figure 1, along with the photomicrographs of the ADSCs at P3 following their isolation from the lipoaspirates obtained from healthy donors using the tumescent technique (Figure 1).

The fingerprints of the common stemness-related membrane proteins were validated using flow cytometry. The results are expressed as the mean \pm SD of the three independent experiments, with * indicating significance at $p \leq 0.05$ (ANOVA followed by Bonferroni's post hoc test), and they confirmed that the stem cell markers CD73 (98.9% \pm 1.03), CD90 (99.9% \pm 0.09), and CD105 (99.8% \pm 0.15) were highly present on the ADSCs' membranes,

whereas the hematopoietic CD34 ($0.82\% \pm 0.34$), and CD45 ($0.087\% \pm 0.03$), and finally CD106 ($0.71\% \pm 0.63$) were not (Figure 2A).

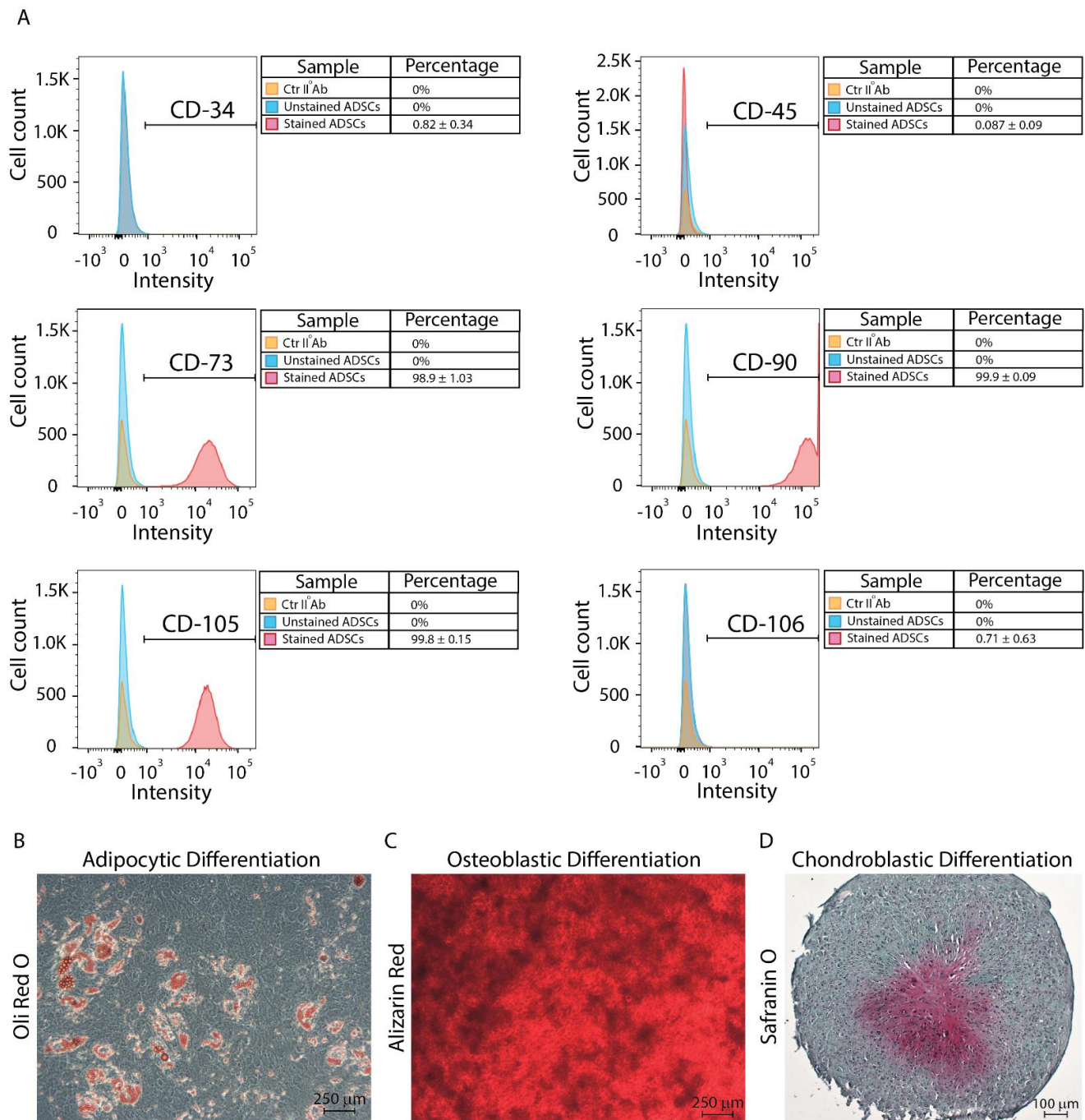


Figure 2. Stemness and differentiation potential assessment. (A) The ADSC stemness was confirmed by verifying the expression of CD73, CD90, and CD105 and the reduced presence of CD34, CD45, and CD106. Differentiation was assessed by inducing the ADSCs through the adipocytic (B), osteoblastic (C), and chondroblastic (D) lineages. Scale bars: 250–100 μ m. Results are expressed as mean \pm SD of three independent experiments. Abbreviations: cluster of differentiation (CD).

The ADSCs were then differentiated through the adipocyte, osteoblastic, and chondroblastic lineages to confirm their multi-lineage potential as a result of three independent experiments. In comparison with the control undifferentiated cells, the differentiated ADSCs developed through the adipocyte lineage, as evidenced by the presence of lipid droplets

revealed by Oil Red O staining (red, Figure 2B). Following their osteoblastic differentiation, the ADSCs were stained with alizarin red, displaying a high level of calcium and, hence, osteoblastic differentiation when compared to the undifferentiated cells (red, Figure 2C). Finally, safranin O staining revealed chondroblastic differentiation in the ADSCs when compared to control cells, indicating the existence of a central core of glycosaminoglycans (violet, GAGs) following three-dimensional chondroblastic differentiation (Figure 2D).

3.2. Implant Morphological Characterization

The SEM micro-photographs revealed a heterogeneous morphology of the surfaces of the implants (Figure 3). The textures of the HA-blasted and bland acid etching implants, as well as the HA-blasted implants with the “new” under-patent treatment, were quite similar, revealing that many HA particles from the blasting treatment adhered to the surface, having a shattered appearance and emerging from the surface. The plasma spray and double-acid-etched surfaces were less irregular than the previous HA-treated surfaces. The surface texture of the laser-treated implant was the most uniform, with occasional voids resembling Howship’s lacunae. (Figure 3). The surface area of the implants, expressed in mm^2 as the mean \pm SD of the three independent experiments, with * indicating significance at $p \leq 0.05$ (ANOVA followed by Bonferroni’s post hoc test), was as follows: plasma spray ($0.097 \text{ mm}^2 \pm 0.004$), laser ($0.108 \text{ mm}^2 \pm 0.01$), HA-blasted and bland acid etching ($0.12 \text{ mm}^2 \pm 0.032$), double acid etching ($0.12 \text{ mm}^2 \pm 0.015$), and HA-blasted “new” ($0.081 \text{ mm}^2 \pm 0.023$) ($p \leq 0.05$).

The micro-architecture of the implants, including the size, distribution, and density of the irregularities, as well as the roughness, is widely acknowledged as having a substantial influence on their mechanical characteristics and interaction with cells [40]. As a result, we analyzed the mean surface particle area, distance, and the spacing between each particle to provide a quantitative measurement of how uniformly the features of interest were distributed across the surface [40] (Figure 4A–E, Table 2).

The results, expressed as the mean \pm SD, of the three independent experiments, with * indicating significance at $p \leq 0.05$ (ANOVA followed by Bonferroni’s post hoc test), showed that the HA-blasted and bland acid etching implants (222 ± 29 , $p \leq 0.05$) had the lowest number of surface particles and, despite having the largest mean area of the surface particles ($20.69 \mu\text{m} \pm 57.53$), did not differ significantly from all the other implants (Figure 4F). The HA-blasted and bland acid etching implants also showed the highest mean distance between particles ($20.69 \mu\text{m} \pm 57.53$, $p \leq 0.05$), the nearest particle distance ($4.49 \mu\text{m} \pm 2.18$, $p \leq 0.05$), and the greatest average wall thickness between particles ($3.13 \mu\text{m} \pm 2.54$, $p \leq 0.05$) (Figure 4G–I).

In addition, according to ISO 4287/2000, we analyzed some well-known surface roughness parameters [13]. Differences in roughness, expressed as the mean \pm SD of three independent experiments, with * indicating significance at $p \leq 0.05$ (ANOVA followed by Bonferroni’s post hoc test), were found between the implants regarding all the parameters, including the arithmetical mean deviation (Ra), root mean square deviation (Rq), skewness of the assessed profile (Rsk), and kurtosis of the assessed profile (Rku).

In the HA-blasted and bland acid etching implants, the parameters of the Ra ($1.16 \mu\text{m} \pm 0.04$) and Rq ($1.72 \mu\text{m} \pm 0.03$, $p \leq 0.05$) (Figure 5H) were the highest with regard to all the other implants ($p \leq 0.05$) (Table 3 and Figure 5G, $p \leq 0.001$). In contrast, the HA-blasted and bland acid etching implant had the lowest values for the roughness-associated parameters, the Rsk and Rku, respectively ($1.48 \mu\text{m} \pm 0.02$ and $2.19 \mu\text{m} \pm 0.07$), differing significantly from all the other implants ($p \leq 0.05$) (Table 3 and Figure 5I,J).

To overcome any issues related to the seeding approach, we report the ratio of the adherent cells retrieved at the three time points to the total number of seeded cells at day zero (1.25×10^6 cells) and the surface area of the implants (Figure 6). The results, expressed as the mean \pm SD of three independent experiments, with * indicating significance at $p \leq 0.001$ (ANOVA followed by Bonferroni’s post hoc test and the paired *t*-test), highlighted the following differences.

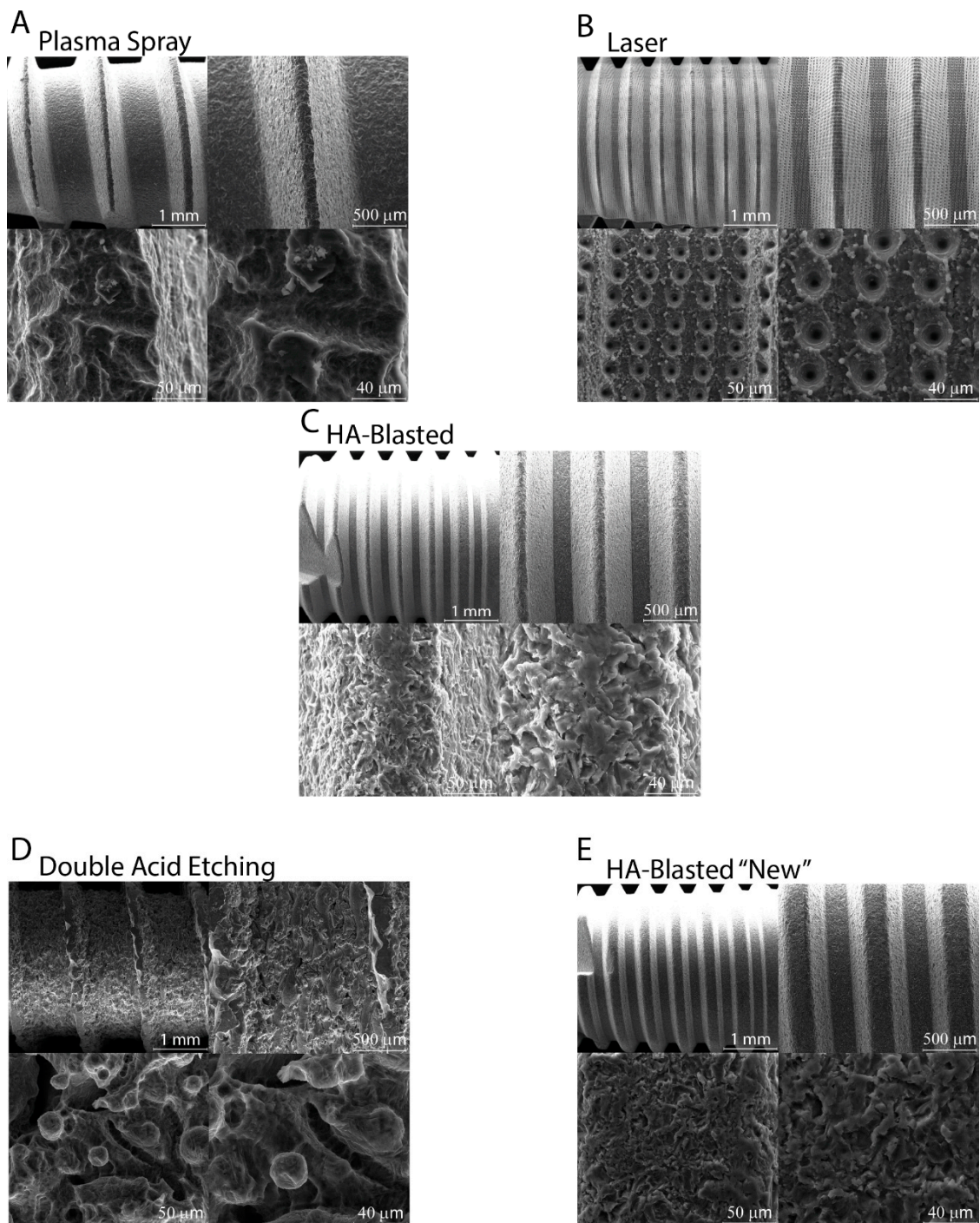


Figure 3. Micro-surface characteristics are presented in the SEM photomicrographs. The surface textures of the HA-blasted and bland-acid-etching implants (C), as well as the HA-blasted implants with the “new” under-patent treatment (E), were highly comparable, suggesting that many HA particles from the blasting process fixed to the surface and became part of it. The plasma spray (A) and double-acid-treated (D) surfaces were less irregular than the previous one. The laser-treated (B) implant exhibited the most uniform surface texture, with regular voids that resembled Howship’s lacunae. Scale bars: 1 mm, 500-50-40 μm.

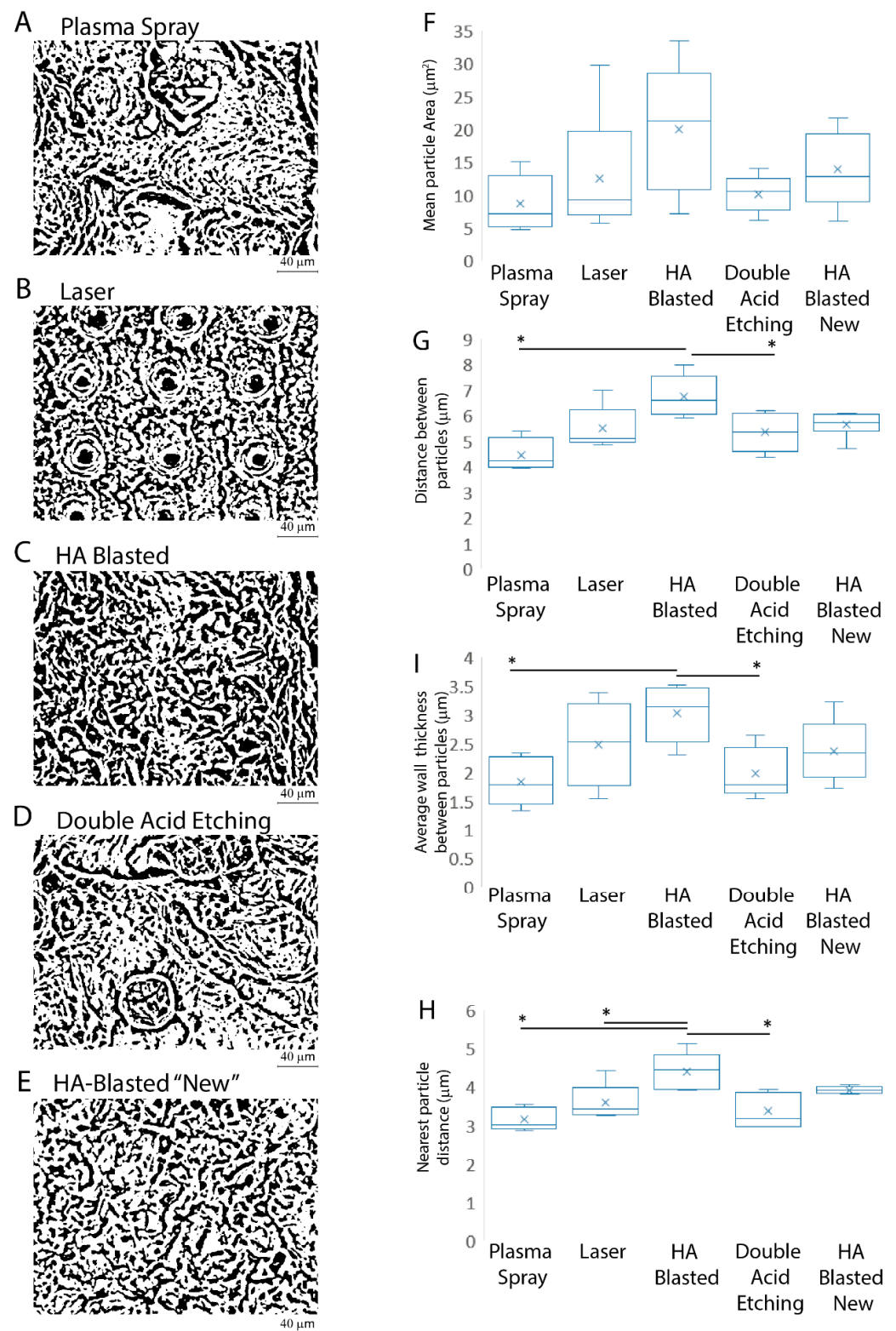


Figure 4. Summary of the surface particle characteristics. The plasma spray (A), laser (B), HA-blasted and bland acid etching (C), double acid etching (D), and HA-blasted “new” (E) implants were analyzed to provide a quantitative measurement of how uniformly the mean surface particle area (F), distance (G), and the spacing between each particle (I) and its closest neighbors’ (H) features of interest were distributed across the surface. Results are expressed as mean \pm SD of three independent experiments, with * indicating significance at $p \leq 0.05$ (ANOVA followed by Bonferroni’s post hoc test).

Table 2. Summary of the surface particle characteristics. The mean surface particle area, distance, and the spacing between each particle and its closest neighbors were analyzed to provide a quantitative measurement of how uniformly the features of interest were distributed across the surface.

	Plasma Spray	Laser	HA-Blasted	Double Acid Etching	HA-Blasted "New"
Particle area (μm^2)	8.59 ± 23.18	11.91 ± 41.22	20.69 ± 57.53	10 ± 22.2	13.19 ± 29.09
Mean distance between particles (μm)	4.55 ± 1.54	5.65 ± 2.16	6.95 ± 2.5	5 ± 1.45	5.8 ± 1.63
Nearest Particle Distance (μm)	3.14 ± 1.27	3.57 ± 1.75	4.49 ± 2.18	3.35 ± 1.27	3.92 ± 1.61
Average Wall Thickness between particles (μm)	1.82 ± 1.37	2.52 ± 2.5	3.13 ± 2.54	1.98 ± 1.51	2.37 ± 1.82
Particles per surface	518 ± 67	316 ± 39	222 ± 29	464 ± 78	337 ± 94

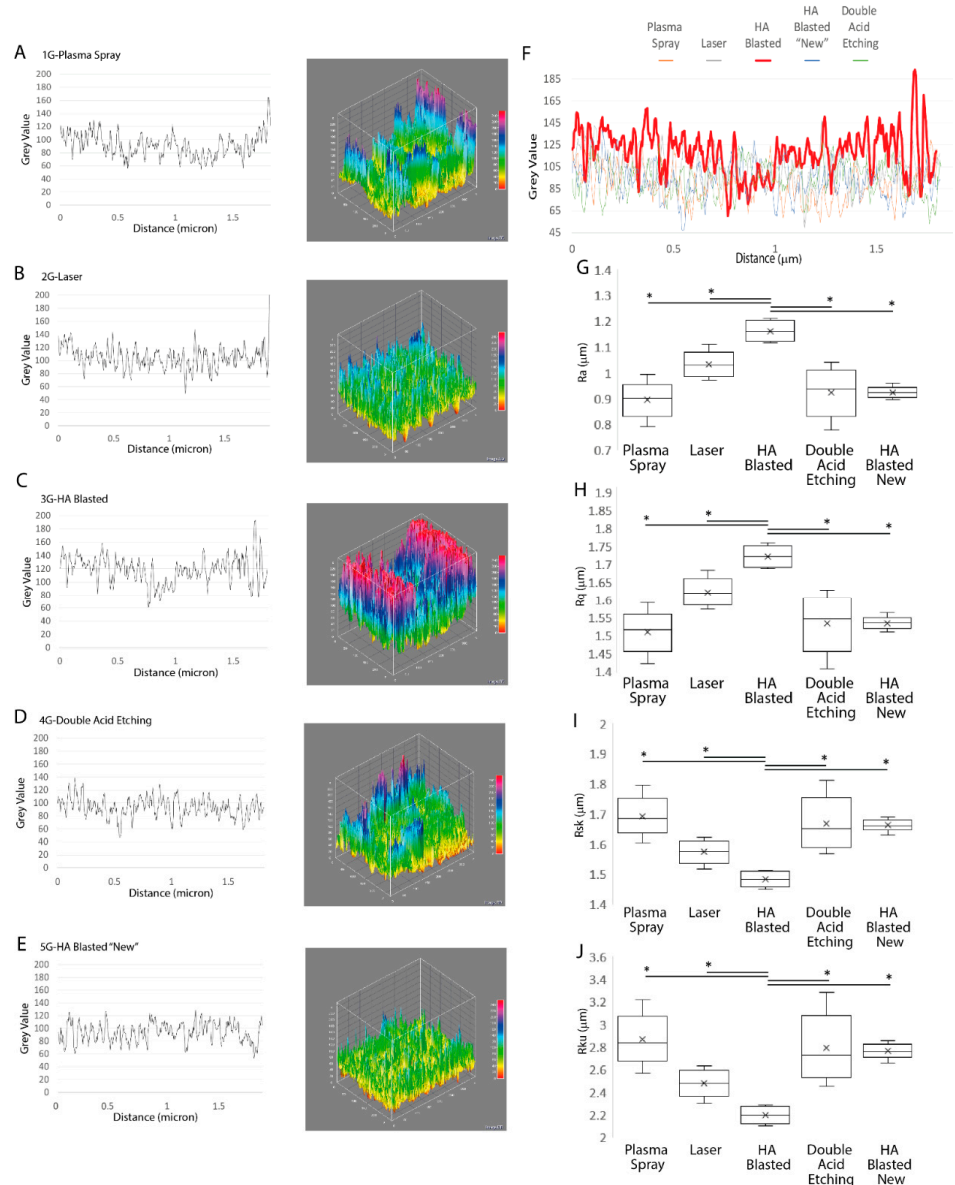


Figure 5. Interfacial roughness profile graphs and 3D profiles. The corresponding roughness profiles of the implants and the specific values used to generate the 3D surface roughness graphs, including

the plasma spray (A), laser (B), HA-blasted and bland acid etching (C), double acid etching (D), and HA-blasted “new” (E) implants, were calculated from the height and distance of the peak profiles in order to highlight the differences in roughness (F) found between the implants’ surfaces tested in this study, including the Ra (G), Ru (H), Rsk (I), and Rku (J). Results are expressed as mean ± SD of three independent experiments, with * indicating significance at $p \leq 0.05$ (ANOVA followed by Fisher’s post hoc test). Abbreviations: arithmetical mean deviation (Ra), root mean square deviation (Rq), skewness of the assessed profile (Rsk), kurtosis of the assessed profile (Rku).

Table 3. Roughness-related parameters analyzed using the ImageJ plugin (sample length 40 μm). Abbreviations: arithmetical mean deviation (Ra), root mean square deviation (Rq), skewness of the assessed profile (Rsk), kurtosis of the assessed profile (Rku).

	Plasma Spray	Laser	HA-Blasted	Double Acid Etching	HA-Blasted New
Ra (μm)	0.89 ± 0.07	1.03 ± 0.05	1.16 ± 0.04	0.92 ± 0.09	0.92 ± 0.02
Rq (μm)	1.5 ± 0.06	1.62 ± 0.04	1.72 ± 0.03	1.53 ± 0.08	1.53 ± 0.02
Rsk (μm)	1.69 ± 0.07	1.57 ± 0.04	1.48 ± 0.02	1.66 ± 0.09	1.66 ± 0.02
Rku (μm)	2.86 ± 0.24	2.47 ± 0.12	2.19 ± 0.07	2.78 ± 0.31	2.76 ± 0.07

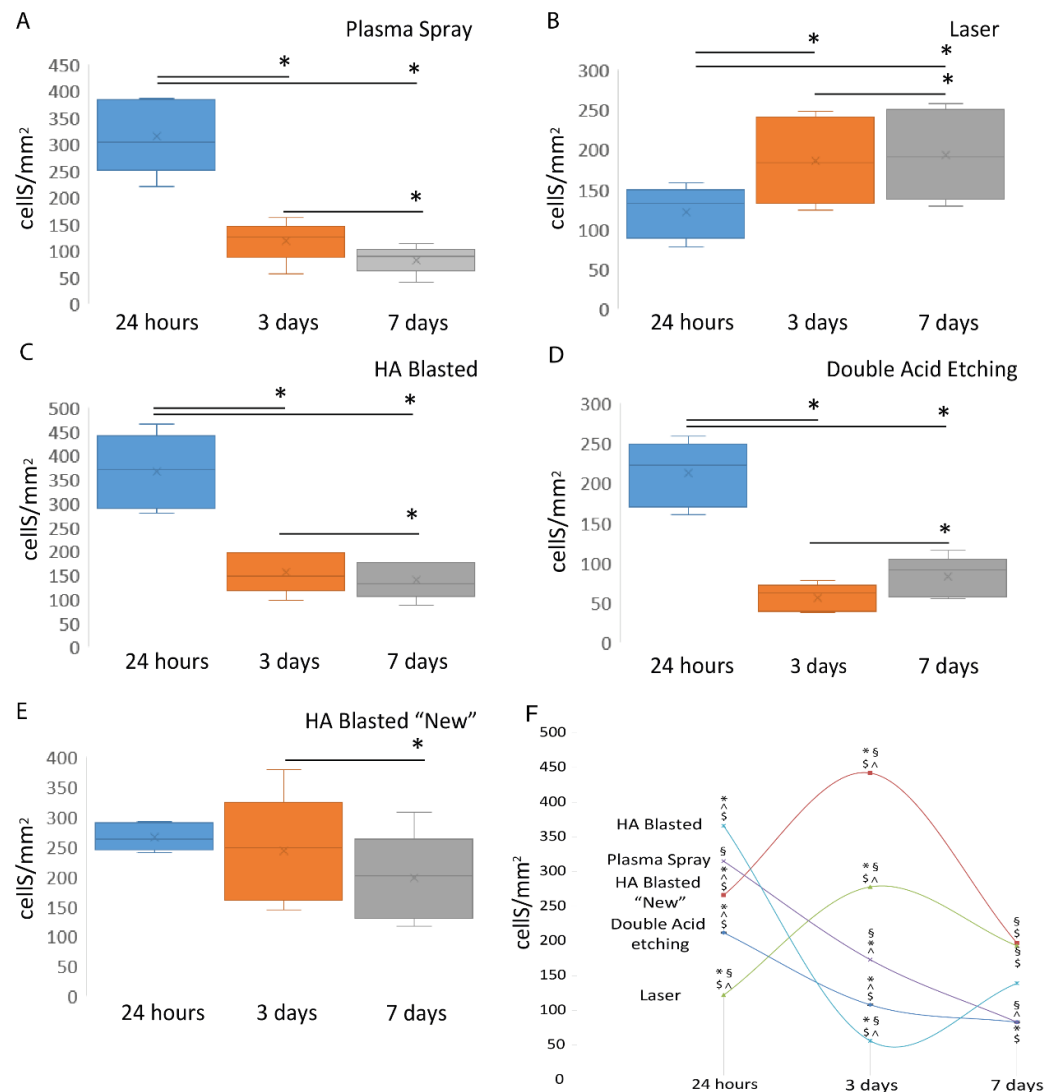


Figure 6. Summary of the ADSCs’ adhesion to the tested dental implants. Graphs of the cell count after 24 h and after three and seven days of the ADSCs’ culture on the whole surface of the commercial

implants, including the plasma spray (A), laser (B), HA-blasted and bland acid etching (C), double acid etching (D) and HA-blasted “new” implants (E). Comparison of the adhesion and proliferation outcomes between the different implants at the same time point (F). Results are expressed as mean ± SD of three independent experiments, with §, *, ^, \$ indicating significance at $p \leq 0.001$ (ANOVA followed by Bonferroni’s post hoc test and paired *t*-test).

Indeed, on day one, the HA-blasted and bland acid etching (366 ± 77 cells/mm²) implants had the highest adhesion, followed by the plasma spray (315 ± 70 cells/mm²), HA-blasted “new” (266 ± 22 cells/mm²), double acid etching (212 ± 40 cells/mm²), and, lastly, laser-treated (122 ± 32 cells/mm²) implants (Figure 6A–E) ($p \leq 0.001$).

By day three, we discovered an increase in the cell number only on the laser-treated (185 ± 55 cells/mm²) implants, whereas the number fell in the case of all the other implants, including the HA-blasted “new” (243 ± 91 cells/mm²), HA-blasted and bland acid etching (155 ± 42 cells/mm²), plasma spray (118 ± 38 cells/mm²), and double acid etching implants (56 ± 17 cells/mm²) (Figure 6A–E) ($p \leq 0.05$).

We discovered a proliferative phase in the double acid etching (83 ± 25 cells/mm²) implants, whereas the laser-treated implants (193 ± 57 cells/mm²) exhibited a constant number of cells, and the HA-blasted “new” (197 ± 74 cells/mm²), HA-blasted and bland acid etching (139 ± 38 cells/mm²) and plasma-spray (83 ± 26 cells/mm²)-treated implants showed a significant reduction in the adhering cell number by day seven (Figure 6A–E) ($p \leq 0.05$).

When the adherent cells were evaluated at the same time point across the different implant surfaces, and the results were expressed as the mean ± SD of the three independent experiments, with §, *, ^, \$ indicating significance at $p \leq 0.001$ (ANOVA followed by Bonferroni’s post hoc test and the paired *t*-test), it was obvious that the plasma-spray-treated surfaces, after 24 h, varied substantially from the laser-treated surface alone ($p < 0.001$), whereas the laser surface was distinct from all the other treated implant surfaces ($p < 0.001$). The HA-blasted and bland acid etching, double acid etching, and HA-blasted “new” treatments differed considerably on all the surfaces except one, which was the plasma spray surface (Figure 6F and Table 4).

Table 4. Comparison of different implants at various time points. An overview of the data analysis comparison of the various implants at different time points. The data are significant with $p \leq 0.001$ (ANOVA followed by Bonferroni’s post hoc test).

Reference Implant	Implant Type	24 h	3 Days	7 Days
Plasma Spray	Laser	<0.001	0.01	<0.001
	HA-Blasted	0.152	0.003	0.125
	Double Acid Etching	0.234	0.054	0.999
	HA-Blasted “New”	0.197	<0.001	<0.001
Laser	Plasma Spray	<0.001	0.01	<0.001
	HA-Blasted	<0.001	<0.001	0.153
	Double Acid Etching	<0.001	0.034	0.049
	HA-Blasted “New”	<0.001	<0.001	999
HA-Blasted	Plasma Spray	0.152	0.003	0.125
	Laser	<0.001	<0.001	0.153
	Double Acid Etching	<0.001	<0.001	0.075
	HA-Blasted “New”	<0.001	<0.001	0.113

Table 4. Cont.

Reference Implant	Implant Type	24 h	3 Days	7 Days
Double Acid Etching	Plasma Spray	0.234	0.054	0.999
	Laser	<0.001	0.034	0.049
	HA-Blasted	<0.001	<0.001	0.075
	HA Blasted “New”	<0.001	<0.001	0.001
HA-Blasted “New”	Plasma Spray	0.197	<0.001	<0.001
	Laser	<0.001	<0.001	0.999
	HA-Blasted	<0.001	<0.001	0.113
	Double Acid Etching	<0.001	<0.001	0.001

At the three-day time point, the plasma spray treatment differed with respect to all but one implant treatment, which was the double acid etching treatment. At the same time point, the laser, HA-blasted and bland acid etching, and the HA-blasted “new” surfaces differed significantly from all the surfaces tested (respectively $p = 0.010$, $p = 0.003$, $p < 0.001$). The double-acid-etched surface differed only from the blasted surfaces ($p < 0.001$) (Figure 6F and Table 4).

Later, on the seventh day, the plasma spray treatment varied considerably from the laser treatment and the HA-blasted “new” treatment ($p < 0.001$) (Figure 6F and Table 4). The laser treatment differed from the plasma spray treatment ($p \leq 0.001$) and the double acid etching treatment ($p = 0.049$). On day seven, the HA-blasted and bland acid etching surface did not vary from any of the treated implants. The HA-blasted “new” treatment diverged from the plasma spray ($p < 0.001$) and double acid etching ($p = 0.001$) treatments, whereas the double acid etching differed solely from the laser ($p = 0.049$) and the HA-blasted “new” treatments ($p = 0.001$) (Figure 6F and Table 4).

3.3. Osteoblastic Induction

To validate the effectiveness of the experimental seeding strategy, we evaluated the expression of various well-known extracellular matrix (ECM) osteoblastic markers, normalizing their values, expressed as the mean \pm SD of three independent experiments, with * indicating significance at $p \leq 0.05$ (ANOVA followed by Bonferroni’s post hoc test), for the adherent cell number and surface area. By increasing the expression of Osn, Coll-I, and ALP with respect to the housekeeping gene in the control cells, all of the treatments and surfaces were able to drive osteoblastic differentiation. The HA-blasted “new” and laser-treated surfaces elicited the greatest ALP and Coll-I expressions when compared to the other implant types at the 24 h time point (Figure 7A,B; Table 5).

By comparison, the greatest Osn expression was achieved under the effects induced by the double-acid-etched surface, while the HA-blasted “new” and laser treatments demonstrated a lower ability to induce Osn (Figure 7D; Table 5). Additionally, Osc was not present in all the samples at 24 h, nor was it present at three days (data not shown).

After three days, the HA-blasted “new”, laser-, and plasma-spray-treated surfaces elicited the greatest ALP, Coll-I, and OSN expressions when compared to the other implant types at the 24 h time point (Figure 7A–C; Table 5). On the contrary, the HA-blasted and bland acid etching and the double acid etching surfaces elicited the smallest production of Osn, ALP, and Coll-I messengers (Figure 7A–C; Table 5).

By day seven, the HA-blasted-“new”-treated surface still elicited the highest levels of Coll-I and OSN, but the laser and plasma spray surfaces exhibited less inductive activity for these extracellular markers (Figure 7A,C; Table 5). The ALP induction reached a similar peak by day seven in the laser and double acid etching implants, while the HA-blasted “new” implant showed a reduced effect on the ALP production (Figure 7A; Table 5). Interestingly, at day seven, even though the HA-blasted and bland acid etching surface was

not as inductive with respect to all the other surfaces, it was the only surface able to induce the late osteoblastic differentiation marker Osc (Figure 7D; Table 5).

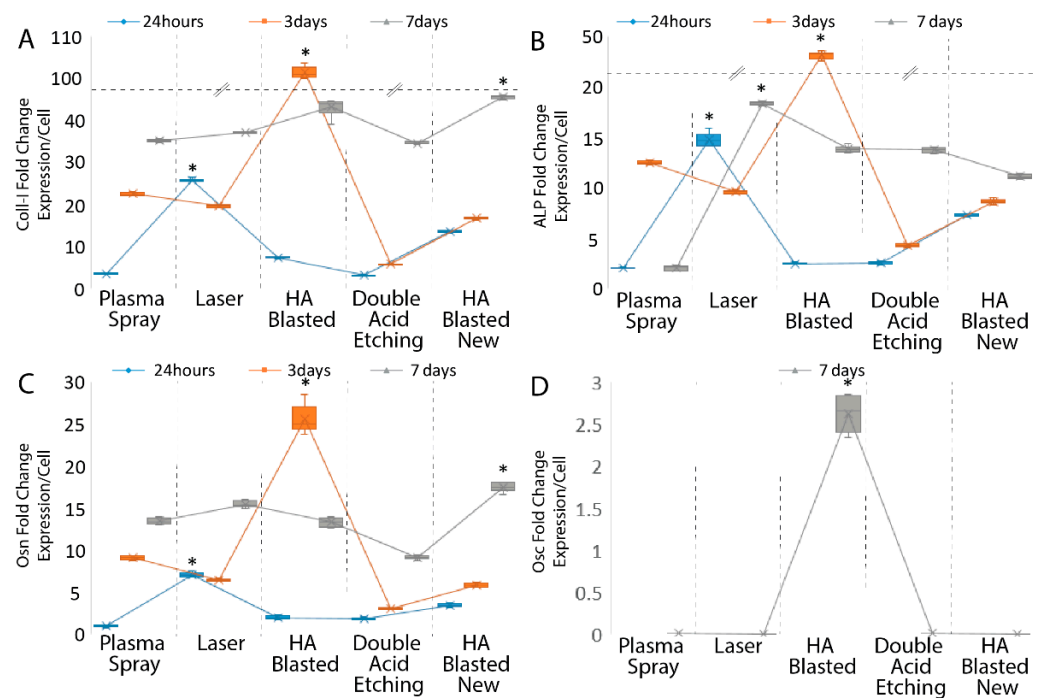


Figure 7. Summary of the ADSC differentiation induction following seeding onto the tested dental implants. Early and late osteoblastic markers, Coll-I (A), ALP (B), Osn (C), and Osc (D), and the expression of ADSCs cultured on the commercially available dental implants after 24 h and three and seven days (A–D). Results are expressed as mean ± SD of three independent experiments, with * indicating significance at $p \leq 0.001$ (ANOVA followed by Bonferroni’s post hoc test). Abbreviations: alkaline phosphatase (ALP); osteocalcin (Osc); osteonectin (Osn); collagen type 1 (Coll-I).

Table 5. Comparison of mRNA expression on different implants at various time points. An overview of the data analysis comparison of the mRNA (ALP, Osn, Coll-I and Osc) expressed by ADSCs on various implants at different time points. Abbreviations: ALP, alkaline phosphatase; Osn, osteonectin; Coll-I, collagen type I; Osc, osteocalcin.

Reference Implant	Implant Type	Coll-I			ALP			Osn		
		24 h	3 days	7 days	24 h	3 days	7 days	24 h	3 days	7 days
Plasma Spray	Laser	<0.001	0.001	<0.001	<0.001	<0.001	<0.001	<0.001	<0.001	<0.001
	HA-Blasted	<0.001	0.002	<0.001	<0.001	<0.001	<0.001	1	<0.001	<0.001
	Double Acid Etching	<0.001	<0.001	<0.001	0.008	<0.001	<0.001	<0.001	<0.001	<0.001
	HA-Blasted “New”	<0.001	0.314	<0.001	0.004	<0.001	<0.001	1	<0.001	<0.001
Laser	Plasma Spray	<0.001	0.001	<0.001	<0.001	<0.001	<0.001	<0.001	<0.001	<0.001
	HA-Blasted	<0.001	<0.001	<0.001	<0.001	<0.001	<0.001	<0.001	<0.001	<0.001
	Double Acid Etching	<0.001	<0.001	1	<0.001	<0.001	<0.001	<0.001	<0.001	<0.001
	HA-Blasted “New”	<0.001	0.025	<0.001	<0.001	0.002	<0.001	<0.001	1	0.022
HA-Blasted	Plasma Spray	<0.001	0.002	<0.001	<0.001	<0.001	<0.001	1	<0.001	<0.001
	Laser	<0.001	<0.001	<0.001	<0.001	<0.001	<0.001	<0.001	<0.001	<0.001
	Double Acid Etching	<0.001	<0.001	<0.001	<0.001	<0.001	<0.001	<0.001	0.218	1
	HA-Blasted “New”	<0.001	<0.001	<0.001	<0.001	<0.001	<0.001	1	<0.001	<0.001

Table 5. Cont.

		Coll-I				ALP		Osn		
Double Acid Etching	Plasma Spray	<0.001	<0.001	<0.001	0.008	<0.001	<0.001	<0.001	<0.001	<0.001
	Laser	<0.001	<0.001	1	<0.001	<0.001	<0.001	<0.001	<0.001	<0.001
	HA-Blasted	<0.001	<0.001	<0.001	<0.001	<0.001	<0.001	<0.001	0.218	1
	HA-Blasted “New”	<0.001	<0.001	<0.001	1	<0.001	<0.001	<0.001	<0.001	<0.001
HA-Blasted “New”	Plasma Spray	<0.001	0.314	<0.001	0.004	<0.001	<0.001	1	<0.001	<0.001
	Laser	<0.001	0.025	<0.001	<0.001	0.002	<0.001	<0.001	1	0.022
	HA-Blasted	<0.001	<0.001	<0.001	<0.001	<0.001	<0.001	1	<0.001	<0.001
	Double Acid Etching	<0.001	<0.001	<0.001	1	<0.001	<0.001	<0.001	<0.001	<0.001

4. Discussion

In simple terms, the effectiveness of dental implants depends on the creation of a barrier that is capable of both sealing the underlying osseous structures and integrating the body of the implant. It is well-known that the tissues interacting with the implant surface are essentially three in number. The first, closely bound to the implant, is poorly cellularized, and its ECM is composed of large and dense bundles of thick Coll-I fibers that contribute to the mechanical resistance and stability of the implants [41,42]. The second is relatively rich in fibroblasts, with a large number of secretory components, and is structurally formed of Coll-I fibers that are heavily associated with collagen type III [41,42]. The third is the bone, which is mostly formed of inorganic mineral material HA with interspersed extracellular proteins, such as Coll-I, Osc, Osn, osteopontin, ALP, and a few scattered osteocytes [41,42].

In this study, we used whole titanium dental implants with moderately rough surfaces, instead of titanium disks [17,20,23,43,44], and ADSCs, chosen because of their ease of separation, as well as their stemness properties [34], to deliver a more realistic approach and to assess the feasibility of a hypothetical combinatorial strategy.

The results revealed that, whereas the topological properties of the implant surfaces under consideration were similar [17,19,25,45], there were substantial differences in the roughness, with the HA-blasted and bland acid etching implants exhibiting the highest value. Furthermore, while the HA-blasted and bland acid etching implants had the fewest surface particles, they also had the lowest density with respect to the other implants.

The stress caused by the mastication loads on a dental implant creates dynamic strains on the surrounding tissues, thus affecting the rehabilitation process [6,14,31]. In view of this, the surface particles and roughness guarantee a differential load transfer depending on their physical and chemical characteristics [6,14,31]. Therefore, the presence of a configuration with the highest roughness and reduced number of particles on the HA-blasted and bland acid etching implants may have a considerably better impact on the adhesion and load transfer during rehabilitation [19,23].

A large body of evidence asserts that many contaminants, being either metallic or nonmetallic, such as C, Mg, Fe, Al, Ca, P, Sr, and F, are introduced onto the implant surface voluntarily (commercially pure titanium grades and titanium alloys) or, in spite of the strict control measures, during the manufacturing process or handling [19,46,47]. We previously demonstrated that machined and laser micro-patterned treatments showed no traceable surface impurity or modification, whereas “sandblasting” introduced elemental traces of C, Fe, Al, and O [48], thus chemically impacting the surface, changing its composition, and influencing the tissue and cell activity [19,46,47]. Another factor that has to be taken into account is the fact that any approach to modifying the surface roughness alters the surface chemistry, finally altering the protein adsorption/adhesion, i.e., Ca²⁺ and Mg²⁺ [12].

As a result, it is possible to hypothesize that the procedures used for HA-blasted and bland acid etching implants modify both the chemical [19,46,47] and topographical

properties, such as the roughness or particle number [19,23], ultimately favoring cell adhesion [12].

Following the initial adhesion, which reached a peak for the HA-blasted and bland acid etching implants, a non-significant proliferative phase occurred for all but one implant, namely, the laser treated implants on day three and the double acid etching implants on day seven. This stands in contrast to previous studies on titanium discs [7,18,20], and it might be due to the low cell density or the whole-body surface via the presence of solubilized metallic ions with negative effects, which cause inflammation and cytotoxicity as their concentration rises [49,50].

On the other hand, the findings suggest that the surface treatment and topography of the whole-body implants (roughness [18,26,27], the surface particle density and characteristics [32], and, potentially, the chemical composition [19,47,50]) have active impacts on ADSC osteoblastic marker synthesis. In support of this view, many studies employing stem cells in vivo and in vitro have found that dental implants [17–21] with moderately rough surfaces allow for better osseointegration [15–29] and reduced marginal bone loss [24,51] compared to smoother or rougher surfaces.

It is known that once cells adhere to biomedical materials, their interaction elicits profound responses within the cells that, depending on how they are perceived, might result in proliferation, differentiation, and, therefore, survival, or apoptosis and, thus, cell death [23,26,27,52–55].

The contact/interaction between the actin cytoskeleton and focal adhesion proteins and the implant surface has been identified as the critical regulator of the integration process [52]. Indeed, the integrin-mediated interaction between the extracellular matrix proteins, such as fibronectin, vitronectin, osteonectin, and collagen-I, and the implant surface has been documented to regulate cell adhesion, differentiation, and survival via programmed cell death (apoptosis) [23,26,27,52–55]. Accordingly, we assume that, following the adhesion, the cytoskeleton of the ADSCs underwent considerable reorganization, resulting in the intracellular signal transmission to the cytoplasm and nucleus [23,52]. The signals, in turn, triggered a variable degree of differentiation, coincident with the expression of increased levels of ALP, Osn, and Coll-I, starting on day one and lasting until day seven. Even though neither the HA-blasted and bland acid etching nor the HA-blasted “new” implants produced significantly more ALP, Osn, or Coll-I than the other treatments, only the HA-blasted and bland acid etching implants could induce the expression of the late osteoblastic marker (Osc). In general, our findings suggest that the surface topography (similar roughness or particle number and distribution) of the HA-treated surfaces promotes the ADSCs’ differentiation and, possibly more, durable osseointegration due to the better load distribution through the surrounding bone during rehabilitation [19,23]. It is also plausible to speculate that the processes utilized for the HA-blasted implants changed the chemical composition of the surface, i.e., by adding Ca^{2+} , P^{5+} , Na^+ , S^{6+} , Si^{4+} , and O^{2-} ions [19,46,47], thus promoting the differentiation of the ADSCs.

5. Conclusions

In summary, we discovered that the surface roughness and treatment composition of dental implants play important roles in the adhesion and differentiation of ADSCs grown on whole-body titanium implants but not in their proliferation.

Significant progress has been achieved in the application of material engineering to the study and modulation of a variety of restorative and pathological disorders [2,56–62], and preclinical attempts have been made to combine material engineering with stem cells [2]. Based on our findings, we suggest that HA-blasted titanium implants combined with adherent ADSCs, which are preconditioned [57,63] to increase their in vivo potential, might be helpful in clinical settings for people with systemic conditions, such as diabetes and osteoporosis [2]. In such a way, it may be feasible to promote quicker osseointegration and increase the patient’s rapid tissue regeneration and bone production, therefore improving their rehabilitation.

However, different seeding concentrations, cytotoxicity tests, longer culture intervals, and pre-clinical studies are still required in order to fully grasp the advantages of HA-blasted implants over the other types and, therefore, to determine the most efficient and suitable surface to employ in conjunction with stem cells.

Author Contributions: Conceptualization, M.M. and F.A.; methodology, F.F., F.A., and R.S.; software, F.F. and R.S.; validation, F.F., F.A., and R.S.; formal analysis, F.F. and R.S.; investigation, F.F., F.A., and R.S.; resources, M.M.; data curation, F.F., F.A., and R.S.; writing—original draft preparation, F.F., F.A., R.S., L.B., and M.M.; writing—review and editing, F.F., F.A., R.S., L.B., and M.M.; visualization, F.F.; supervision, M.M.; project administration, M.M.; funding acquisition, M.M. All authors have read and agreed to the published version of the manuscript.

Funding: The study was self-supported by the Department of Medical, Surgery and Health Sciences of the University of Trieste.

Institutional Review Board Statement: The study was conducted in accordance with the Declaration of Helsinki, and the ADSCs samples were taken after approval from the independent ethics committee of the Azienda Ospedaliero—Universitaria of Udine (Parere N. 103/2011/Sper).

Informed Consent Statement: Informed consent was obtained from all subjects involved in the study and all clinical investigations have been conducted according to the principles expressed in the Declaration of Helsinki.

Data Availability Statement: The datasets generated and/or analyzed during the current study are available upon reasonable request from the corresponding author.

Conflicts of Interest: The authors declare no conflict of interest.

Abbreviations

Adipose-tissue-derived stem cells (ADSCs), hydroxyapatite (HA), collagen type I (Coll-I), osteonectin (Osn), alkaline phosphatase (ALP), osteocalcin (Osc), arithmetical mean of the roughness area (Sa), fetal bovine serum (FBS), epithelial growth factor (EGF), bland detaching solution (CTC), cluster of differentiation stem markers (CD), DMEM high glucose (HG), transforming growth factor-3 (TGF β -3), scanning electron microscope (SEM), root mean square deviation (Rq), skewness of the assessed profile (Rsk), kurtosis of the assessed profile (Rku), arithmetical mean deviation (Ra), HA-blasted and bland acid etching (HA-blasted), and extracellular matrix (ECM).

References

1. Dental Implants Market Size. Share & Trends Analysis Report by Type (Titanium, Zirconium), by Region (North America, Europe, Asia Pacific, Latin America, MEA), and Segment Forecasts, 2020–2027. Available online: <https://www.marketresearch.com/Grand-View-Research-v4060/Dental-Implant-Size-Share-Trends-14163164/> (accessed on 25 July 2022).
2. Duan, Y.; Ma, W.; Li, D.; Wang, T.; Liu, B. Enhanced Osseointegration of Titanium Implants in a Rat Model of Osteoporosis Using Multilayer Bone Mesenchymal Stem Cell Sheets. *Exp. Ther. Med.* **2017**, *14*, 5717–5726. [[CrossRef](#)] [[PubMed](#)]
3. Albrektsson, T.; Brånemark, P.I.; Hansson, H.A.; Lindström, J. Osseointegrated Titanium Implants. Requirements for Ensuring a Long-Lasting, Direct Bone-to-Implant Anchorage in Man. *Acta Orthop. Scand.* **1981**, *52*, 155–170. [[CrossRef](#)] [[PubMed](#)]
4. Coelho, P.G.; Granjeiro, J.M.; Romanos, G.E.; Suzuki, M.; Silva, N.R.F.; Cardaropoli, G.; Thompson, V.P.; Lemons, J.E. Basic Research Methods and Current Trends of Dental Implant Surfaces. *J. Biomed. Mater. Res. B Appl. Biomater.* **2009**, *88*, 579–596. [[CrossRef](#)] [[PubMed](#)]
5. Insua, A.; Monje, A.; Wang, H.-L.; Miron, R.J. Basis of Bone Metabolism around Dental Implants during Osseointegration and Peri-Implant Bone Loss. *J. Biomed. Mater. Res. A* **2017**, *105*, 2075–2089. [[CrossRef](#)] [[PubMed](#)]
6. Li, J.; Jansen, J.A.; Walboomers, X.F.; van den Beucken, J.J. Mechanical Aspects of Dental Implants and Osseointegration: A Narrative Review. *J. Mech. Behav. Biomed. Mater.* **2020**, *103*, 103574. [[CrossRef](#)]
7. Guida, L.; Annunziata, M.; Rocci, A.; Contaldo, M.; Rullo, R.; Oliva, A. Biological Response of Human Bone Marrow Mesenchymal Stem Cells to Fluoride-Modified Titanium Surfaces. *Clin. Oral Implant. Res.* **2010**, *21*, 1234–1241. [[CrossRef](#)]
8. Qahash, M.; Susin, C.; Polimeni, G.; Hall, J.; Wikesjö, U.M.E. Bone Healing Dynamics at Buccal Peri-Implant Sites. *Clin. Oral Implant. Res.* **2008**, *19*, 166–172. [[CrossRef](#)]
9. Ripamonti, U.; Roden, L.C.; Ferretti, C.; Klar, R.M. Biomimetic Matrices Self-Initiating the Induction of Bone Formation. *J. Craniofacial Surg.* **2011**, *22*, 1859–1870. [[CrossRef](#)]

10. Löberg, J.; Gretzer, C.; Mattisson, I.; Ahlberg, E. Electronic Properties of Anodized TiO₂ Electrodes and the Effect on in Vitro Response. *J. Biomed. Mater. Res. B Appl. Biomater.* **2014**, *102*, 826–839. [[CrossRef](#)]
11. Vandrovцова, M.; Tolde, Z.; Vanek, P.; Nehasil, V.; Doubková, M.; Trávníčková, M.; Drahokoupil, J.; Buixaderas, E.; Borodavka, F.; Novakova, J.; et al. Beta-Titanium Alloy Covered by Ferroelectric Coating—Physicochemical Properties and Human Osteoblast-Like Cell Response. *Coatings* **2021**, *11*, 210. [[CrossRef](#)]
12. Barberi, J.; Spriano, S. Titanium and Protein Adsorption: An Overview of Mechanisms and Effects of Surface Features. *Materials* **2021**, *14*, 1590. [[CrossRef](#)]
13. Martinez, M.A.F.; de Fátima Balderrama, Í.; Karam, P.S.B.H.; de Oliveira, R.C.; de Oliveira, F.A.; Grandini, C.R.; Vicente, F.B.; Stavropoulos, A.; Zangrando, M.S.R.; Sant’Ana, A.C.P. Surface Roughness of Titanium Disks Influences the Adhesion, Proliferation and Differentiation of Osteogenic Properties Derived from Human. *Int. J. Implant Dent.* **2020**, *6*, 46. [[CrossRef](#)]
14. Kassem, R.; Samara, A.; Biadsee, A.; Masarwa, S.; Mtanis, T.; Ormianer, Z. A Comparative Evaluation of the Strain Transmitted through Prostheses on Implants with Two Different Macro-Structures and Connection during Insertion and Loading Phase: An In Vitro Study. *Materials* **2022**, *15*, 4954. [[CrossRef](#)]
15. Albrektsson, T.; Wennerberg, A. Oral Implant Surfaces: Part 1—Review Focusing on Topographic and Chemical Properties of Different Surfaces and in Vivo Responses to Them. *Int. J. Prosthodont.* **2004**, *17*, 536–543. [[PubMed](#)]
16. Albrektsson, T.; Wennerberg, A. Oral Implant Surfaces: Part 2—Review Focusing on Clinical Knowledge of Different Surfaces. *Int. J. Prosthodont.* **2004**, *17*, 544–564. [[PubMed](#)]
17. Cipriano, A.F.; De Howitt, N.; Gott, S.C.; Miller, C.; Rao, M.P.; Liu, H. Bone Marrow Stromal Cell Adhesion and Morphology on Micro- and Sub-Micropatterned Titanium. *J. Biomed. Nanotechnol.* **2014**, *10*, 660–668. [[CrossRef](#)] [[PubMed](#)]
18. Zanicotti, D.G.; Duncan, W.J.; Seymour, G.J.; Coates, D.E. Effect of Titanium Surfaces on the Osteogenic Differentiation of Human Adipose-Derived Stem Cells. *Int. J. Oral Maxillofac. Implant.* **2018**, *33*, e77–e87. [[CrossRef](#)] [[PubMed](#)]
19. Albrektsson, T.; Wennerberg, A. On Osseointegration in Relation to Implant Surfaces. *Clin. Implant. Dent. Relat. Res.* **2019**, *21* (Suppl. S1), 4–7. [[CrossRef](#)]
20. Annunziata, M.; Guida, L.; Perillo, L.; Aversa, R.; Passaro, I.; Oliva, A. Biological Response of Human Bone Marrow Stromal Cells to Sandblasted Titanium Nitride-Coated Implant Surfaces. *J. Mater. Sci. Mater. Med.* **2008**, *19*, 3585–3591. [[CrossRef](#)]
21. Giner, L.; Mercadé, M.; Torrent, S.; Punset, M.; Pérez, R.A.; Delgado, L.M.; Gil, F.J. Double Acid Etching Treatment of Dental Implants for Enhanced Biological Properties. *J. Appl. Biomater. Funct. Mater.* **2018**, *16*, 83–89. [[CrossRef](#)]
22. Rosa, M.B.; Albrektsson, T.; Francischone, C.E.; Schwartz Filho, H.O.; Wennerberg, A. The Influence of Surface Treatment on the Implant Roughness Pattern. *J. Appl. Oral Sci.* **2012**, *20*, 550–555. [[CrossRef](#)] [[PubMed](#)]
23. Kulangara, K.; Yang, J.; Chellappan, M.; Yang, Y.; Leong, K.W. Nanotopography Alters Nuclear Protein Expression, Proliferation and Differentiation of Human Mesenchymal Stem/Stromal Cells. *PLoS ONE* **2014**, *9*, e114698. [[CrossRef](#)] [[PubMed](#)]
24. Zheng, G.; Guan, B.; Hu, P.; Qi, X.; Wang, P.; Kong, Y.; Liu, Z.; Gao, P.; Li, R.; Zhang, X.; et al. Topographical Cues of Direct Metal Laser Sintering Titanium Surfaces Facilitate Osteogenic Differentiation of Bone Marrow Mesenchymal Stem Cells through Epigenetic Regulation. *Cell Prolif.* **2018**, *51*, e12460. [[CrossRef](#)] [[PubMed](#)]
25. Albouy, J.-P.; Abrahamsson, I.; Persson, L.G.; Berglundh, T. Implant Surface Characteristics Influence the Outcome of Treatment of Peri-Implantitis: An Experimental Study in Dogs. *J. Clin. Periodontol.* **2011**, *38*, 58–64. [[CrossRef](#)] [[PubMed](#)]
26. Abagnale, G.; Steger, M.; Nguyen, V.H.; Hersch, N.; Sechi, A.; Jousen, S.; Denecke, B.; Merkel, R.; Hoffmann, B.; Dreser, A.; et al. Surface Topography Enhances Differentiation of Mesenchymal Stem Cells towards Osteogenic and Adipogenic Lineages. *Biomaterials* **2015**, *61*, 316–326. [[CrossRef](#)]
27. Steger, M.; Abagnale, G.; Bremus-Köbberling, E.; Wagner, W.; Gillner, A. Nanoscale Biofunctionalization of Polymer Surfaces by Laser Treatment for Controlled Cellular Differentiation. In *Optically Induced Nanostructures: Biomedical and Technical Applications*; König, K., Ostendorf, A., Eds.; Walter de Gruyter Inc.: Berlin, Germany; Boston, MA, USA, 2015.
28. Svanborg, L.M.; Andersson, M.; Wennerberg, A. Surface Characterization of Commercial Oral Implants on the Nanometer Level. *J. Biomed. Mater. Res. B Appl. Biomater.* **2010**, *92*, 462–469. [[CrossRef](#)]
29. Wennerberg, A.; Ide-Ektessabi, A.; Hatkamata, S.; Sawase, T.; Johansson, C.; Albrektsson, T.; Martinelli, A.; Södervall, U.; Odelius, H. Titanium Release from Implants Prepared with Different Surface Roughness. *Clin. Oral Implant. Res.* **2004**, *15*, 505–512. [[CrossRef](#)]
30. Wang, L.; Aghvami, M.; Brunski, J.; Helms, J. Biophysical Regulation of Osteotomy Healing: An Animal Study. *Clin. Implant Dent. Relat. Res.* **2017**, *19*, 590–599. [[CrossRef](#)]
31. Leucht, P.; Kim, J.-B.; Wazen, R.; Currey, J.A.; Nanci, A.; Brunski, J.B.; Helms, J.A. Effect of Mechanical Stimuli on Skeletal Regeneration around Implants. *Bone* **2007**, *40*, 919–930. [[CrossRef](#)]
32. Wang, L.; Wu, Y.; Perez, K.C.; Hyman, S.; Brunski, J.B.; Tulu, U.; Bao, C.; Salmon, B.; Helms, J.A. Effects of Condensation on Peri-Implant Bone Density and Remodeling. *J. Dent. Res.* **2017**, *96*, 413–420. [[CrossRef](#)]
33. Kotsovilis, S.; Karoussis, I.K.; Fourmouis, I. A Comprehensive and Critical Review of Dental Implant Placement in Diabetic Animals and Patients. *Clin. Oral Implant. Res.* **2006**, *17*, 587–599. [[CrossRef](#)] [[PubMed](#)]
34. Ferro, F.; Spelat, R.; Falini, G.; Gallelli, A.; D’Aurizio, F.; Puppato, E.; Pandolfi, M.; Beltrami, A.P.; Cesselli, D.; Beltrami, C.A.; et al. Adipose Tissue-Derived Stem Cell In Vitro Differentiation in a Three-Dimensional Dental Bud Structure. *Am. J. Pathol.* **2011**, *178*, 2299–2310. [[CrossRef](#)] [[PubMed](#)]

35. Lee, J.A.; Parrett, B.M.; Conejero, J.A.; Laser, J.; Chen, J.; Kogon, A.J.; Nanda, D.; Grant, R.T.; Breitbart, A.S. Biological Alchemy: Engineering Bone and Fat from Fat-Derived Stem Cells. *Ann. Plast. Surg.* **2003**, *50*, 610–617. [[CrossRef](#)]
36. Hattori, H.; Masuoka, K.; Sato, M.; Ishihara, M.; Asazuma, T.; Takase, B.; Kikuchi, M.; Nemoto, K.; Ishihara, M. Bone Formation Using Human Adipose Tissue-Derived Stromal Cells and a Biodegradable Scaffold. *J. Biomed. Mater. Res. B Appl. Biomater.* **2006**, *76*, 230–239. [[CrossRef](#)] [[PubMed](#)]
37. Hicok, K.C.; Du Laney, T.V.; Zhou, Y.S.; Halvorsen, Y.-D.C.; Hitt, D.C.; Cooper, L.F.; Gimble, J.M. Human Adipose-Derived Adult Stem Cells Produce Osteoid in Vivo. *Tissue Eng.* **2004**, *10*, 371–380. [[CrossRef](#)]
38. Nicholson, J.W. Titanium Alloys for Dental Implants: A Review. *Prosthesis* **2020**, *2*, 100–116. [[CrossRef](#)]
39. Hasegawa, M.; Saruta, J.; Hirota, M.; Taniyama, T.; Sugita, Y.; Kubo, K.; Ishijima, M.; Ikeda, T.; Maeda, H.; Ogawa, T. A Newly Created Meso-, Micro-, and Nano-Scale Rough Titanium Surface Promotes Bone-Implant Integration. *Int. J. Mol. Sci.* **2020**, *21*, 783. [[CrossRef](#)]
40. Haeri, M.; Haeri, M. ImageJ Plugin for Analysis of Porous Scaffolds Used in Tissue Engineering. *J. Open Res. Softw.* **2015**, *3*, e1. [[CrossRef](#)]
41. Zhang, B.; Li, J.; He, L.; Huang, H.; Weng, J. Bio-Surface Coated Titanium Scaffolds with Cancellous Bone-like Biomimetic Structure for Enhanced Bone Tissue Regeneration. *Acta Biomater.* **2020**, *114*, 431–448. [[CrossRef](#)]
42. Ehrenfest, D.M.D.; Piattelli, A.; Sammartino, G.; Wang, H.-L. New Biomaterials and Regenerative Medicine Strategies in Periodontology, Oral Surgery, Esthetic and Implant Dentistry 2018. *Biomed. Res. Int.* **2019**, *2019*, 1363581. [[CrossRef](#)]
43. Klein, M.O.; Bijelic, A.; Ziebart, T.; Koch, F.; Kämmerer, P.W.; Wieland, M.; Konerding, M.A.; Al-Nawas, B. Submicron Scale-Structured Hydrophilic Titanium Surfaces Promote Early Osteogenic Gene Response for Cell Adhesion and Cell Differentiation. *Clin. Implant Dent. Relat. Res.* **2013**, *15*, 166–175. [[CrossRef](#)] [[PubMed](#)]
44. Wennerberg, A.; Albrektsson, T. On Implant Surfaces: A Review of Current Knowledge and Opinions. *Int. J. Oral Maxillofac. Implant.* **2010**, *25*, 63–74.
45. Albouy, J.-P.; Abrahamsson, I.; Berglundh, T. Spontaneous Progression of Experimental Peri-Implantitis at Implants with Different Surface Characteristics: An Experimental Study in Dogs. *J. Clin. Periodontol.* **2012**, *39*, 182–187. [[CrossRef](#)] [[PubMed](#)]
46. Nishiguchi, S.; Kato, H.; Neo, M.; Oka, M.; Kim, H.M.; Kokubo, T.; Nakamura, T. Alkali- and Heat-Treated Porous Titanium for Orthopedic Implants. *J. Biomed. Mater. Res.* **2001**, *54*, 198–208. [[CrossRef](#)]
47. Dhaliwal, J.S.; David, S.R.N.; Zulhilmi, N.R.; Sodhi Dhaliwal, S.K.; Knights, J.; de Albuquerque Junior, R.F. Contamination of Titanium Dental Implants: A Narrative Review. *SN Appl. Sci.* **2020**, *2*, 1011. [[CrossRef](#)]
48. Faccioni, F.; Bevilacqua, L.; Porrelli, D.; Khoury, A.; Faccioni, P.; Turco, G.; Frassetto, A.; Maglione, M. Ultrasonic Instrument Effects on Different Implant Surfaces: Profilometry, Energy-Dispersive X-Ray Spectroscopy, and Microbiology In Vitro Study. *Int. J. Oral Maxillofac. Implant.* **2021**, *36*, 520–528. [[CrossRef](#)]
49. Zhang, J.; Cai, B.; Tan, P.; Wang, M.; Abotaleb, B.; Zhu, S.; Jiang, N. Promoting Osseointegration of Titanium Implants through Magnesium- and Strontium-Doped Hierarchically Structured Coating. *J. Mater. Res. Technol.* **2022**, *16*, 1547–1559. [[CrossRef](#)]
50. Stricker, A.; Bergfeldt, T.; Fretwurst, T.; Addison, O.; Schmelzeisen, R.; Rothweiler, R.; Nelson, K.; Gross, C. Impurities in Commercial Titanium Dental Implants—A Mass and Optical Emission Spectrometry Elemental Analysis. *Dent. Mater.* **2022**, *38*, 1395–1403. [[CrossRef](#)]
51. Kämmerer, P.W.; Pabst, A.M.; Dau, M.; Staedt, H.; Al-Nawas, B.; Heller, M. Immobilization of BMP-2, BMP-7 and Alendronic Acid on Titanium Surfaces: Adhesion, Proliferation and Differentiation of Bone Marrow-Derived Stem Cells. *J. Biomed. Mater. Res. A* **2020**, *108*, 212–220. [[CrossRef](#)]
52. Feller, L.; Jadwat, Y.; Khammissa, R.A.G.; Meyerov, R.; Schechter, I.; Lemmer, J. Cellular Responses Evoked by Different Surface Characteristics of Intraosseous Titanium Implants. *Biomed. Res. Int.* **2015**, *2015*, 171945. [[CrossRef](#)]
53. Geiger, B.; Bershadsky, A.; Pankov, R.; Yamada, K.M. Transmembrane Crosstalk between the Extracellular Matrix–Cytoskeleton Crosstalk. *Nat. Rev. Mol. Cell Biol.* **2001**, *2*, 793–805. [[CrossRef](#)] [[PubMed](#)]
54. Cukierman, E.; Pankov, R.; Yamada, K.M. Cell Interactions with Three-Dimensional Matrices. *Curr. Opin. Cell Biol.* **2002**, *14*, 633–639. [[CrossRef](#)]
55. Wozniak, M.A.; Modzelewska, K.; Kwong, L.; Keely, P.J. Focal Adhesion Regulation of Cell Behavior. *Biochim. Biophys. Acta* **2004**, *1692*, 103–119. [[CrossRef](#)] [[PubMed](#)]
56. Xu, B.; Zhang, J.; Brewer, E.; Tu, Q.; Yu, L.; Tang, J.; Krebsbach, P.; Wieland, M.; Chen, J. Osterix Enhances BMSC-Associated Osseointegration of Implants. *J. Dent. Res.* **2009**, *88*, 1003–1007. [[CrossRef](#)] [[PubMed](#)]
57. Ferro, F.; Spelat, R.; Shaw, G.; Coleman, C.M.; Chen, X.Z.; Connolly, D.; Palamá, E.M.F.; Gentili, C.; Contessotto, P.; Murphy, M.J. Regenerative and Anti-Inflammatory Potential of Regularly Fed, Starved Cells and Extracellular Vesicles In Vivo. *Cells* **2022**, *11*, 2696. [[CrossRef](#)]
58. Spelat, R.; Ferro, F.; Contessotto, P.; Warren, N.J.; Marsico, G.; Armes, S.P.; Pandit, A. A Worm Gel-Based 3D Model to Elucidate the Paracrine Interaction between Multiple Myeloma and Mesenchymal Stem Cells. *Mater. Today Bio* **2020**, *5*, 100040. [[CrossRef](#)]
59. Contessotto, P.; Pandit, A. Therapies to Prevent Post-Infarction Remodelling: From Repair to Regeneration. *Biomaterials* **2021**, *275*, 120906. [[CrossRef](#)]
60. Mayerhofer, C.C.K.; Ueland, T.; Broch, K.; Vincent, R.P.; Cross, G.F.; Dahl, C.P.; Aukrust, P.; Gullestad, L.; Hov, J.R.; Trøseid, M. Increased Secondary/Primary Bile Acid Ratio in Chronic Heart Failure. *J. Card. Fail.* **2017**, *23*, 666–671. [[CrossRef](#)]

61. Marsico, G.; Jin, C.; Abbah, S.A.; Brauchle, E.M.; Thomas, D.; Rebelo, A.L.; Orbanić, D.; Chantepie, S.; Contessotto, P.; Papy-Garcia, D.; et al. Elastin-like Hydrogel Stimulates Angiogenesis in a Severe Model of Critical Limb Ischemia (CLI): An Insight into the Glyco-Host Response. *Biomaterials* **2021**, *269*, 120641. [[CrossRef](#)]
62. Limongi, T.; Brigo, L.; Tirinato, L.; Pagliari, F.; Gandin, A.; Contessotto, P.; Giugni, A.; Brusatin, G. Three-Dimensionally Two-Photon Lithography Realized Vascular Grafts. *Biomed. Mater.* **2021**, *16*, 035013. [[CrossRef](#)]
63. Ferro, F.; Spelat, R.; Shaw, G.; Duffy, N.; Islam, M.N.; O'Shea, P.M.; O'Toole, D.; Howard, L.; Murphy, J.M. Survival/Adaptation of Bone Marrow-Derived Mesenchymal Stem Cells After Long-Term Starvation Through Selective Processes. *Stem Cells* **2019**, *37*, 813–827. [[CrossRef](#)] [[PubMed](#)]